QUASI-STEADY-STATE REDUCTION OF A MODEL FOR CYTOPLASMIC TRANSPORT OF SECRETORY VESICLES IN STIMULATED CHROMAFFIN CELLS

DIETMAR OELZ

Abstract. Neurosecretory cells spatially redistribute their pool of secretory vesicles upon stimulation. Recent observations suggest that in chromaffin cells vesicles move either freely or in a directed fashion by what appears to be a conveyor belt mechanism. We suggest that this observation reflects the transient active transport through molecular motors along cytoskeleton fibres and quantify this effect using a 1D mathematical model that couples a diffusion equation to advection equations. In agreement with recent observations the model predicts that random motion dominates towards the cell centre whereas directed motion prevails in the region abutting the cortical membrane.

Furthermore the model explains the observed bias of directed transport towards the periphery upon stimulation. Our model suggests that even if vesicle transport is indifferent with respect to direction, stimulation creates a gradient of free vesicles at first and this triggers the bias of transport in forward direction. Using matched asymptotic expansion we derive an approximate drift-diffusion type model that is capable of quantifying this effect. Based on this model we compute the characteristic time for the system to adapt to secretagogue stimulation and we identify a Michaelis-Menten-type law describing the flux of vesicles entering the pathway to exocytosis.

1. Introduction

Neuroendocrine chromaffin cells in the adrenal medulla are a model system to study the exocytosis of secretory vesicles (SVs) as well as their transport from the site of biosynthesis at the Golgi apparatus towards the site of exocytosis [8]. Vesicle transport is driven by molecular motor proteins which drag vesicles along cytoskeleton fibres [2]. Studies with cytoskeleton inhibiting drugs have shown that both microtubules and actin filaments are involved in the cytoplasmic transport of these secretory granules [5, 14].

Especially in the perinuclear region both cytoskeleton systems contribute to the transport of secretory vesicles [6, 23]. In the periphery of the cell, however, transport along the actin filament network through molecular motors such as myosin-V [19, 20] dominates [1, 8].

Microtubules are mostly aligned radially while in the cortical region their density is lower and they align tangentially with the cortex [23]. Recently, our understanding of the role of the actin cortex has shifted [10]. Historically it has been considered a barrier which limits and controls the access of the SVs to the site of exocytosis [22]. More recently it is attributed an active role: It contributes to the transport of SVs in the subcortical region [18], facilitates the motion of SV through the cellular cortex towards the secretory sites and it mechanically supports the mechanical process of exocytosis [9].

Tracking of secretory granules in time-lapse confocal imaging has revealed that upon secretagogue stimulation cells spatially adjust their secretory vesicle pools. Upon stimulation directed motion in the subcortical region abutting the cortical actin network is biased towards the cortex which helps to replenish the pools of releasable vesicles [14]. The feedback mechanisms which trigger this bias, however, are elusive.

The aim of this study is to introduce a quantitative description of secretory vesicle transport in chromaffin cells and to answer the question whether active feedback mechanisms are responsible for the switch in transport characteristics upon stimulation, or whether this adaption can be explained as a global phenomenon which emerges from the local interplay of molecular motors with cargo vesicles and cytoskeleton tracks.

Models and simulations of intra-cellular transport have so far focused on transport along and within bundles of fibres, but the modelling of cytoplasmic vesicle transport as part of the secretory pathway has only received minor attention from modellers so far: The chemical reaction network underlying exocytosis has been modelled through a system of rate equations in [7]. Agent based models have been formulated and simulated in various studies, namely in [15] focusing on simulation methods, in [13] considering spatial aspects of vesicular sorting into different compartments and in [3] in order to investigate the emergence of patterns.

Studies which link mechanistic models of cytoplasmic transport to the statistics of excytosis are scarce. One example is [12] in which simulations of stochastic differential equations are used to show that directed transport in principle can explain non-Poissonian vesicle release statistics.

In the spirit of a wide range of models considering bidirectional transport along cytoskeleton fibres [21, 4], we introduce a PDE-type (partial differential equation) mean field model for cytoplasmic vesicle transport along a diverse population of fibre tracks. We also report a simpler drift-diffusion model which we derive as a leading order approximation to the system of PDEs [16, 4]. Since in our model secretory vesicles bind upon stimulation to the actin cortex representing the boundary of the domain we also include the boundary layers in the asymptotic analysis, i.e. we perform matched asymptotic expansion and derive a limit solution composed of solutions to the boundary layer problems and the inner problem.

It is our goal to identify parameter regimes which explain the adaption of intracellular transport to secretagogue stimulation. It should be noted that a wide range of models could possibly be used to address these questions ranging from Markov chains modellling the transition between vesicle compartments to detailed simulations. The 1D PDE model we present here provides an intermediate level of abstraction and we regard it as both, a refinement of transition-rate compartment models and as a proof of concept and guideline to facilitate parameter estimation for detailed agent based simulations.

The structure of this paper is as follows. In section 2 we will introduce the mathematical model, then in section 3 we will re-express the model through symmetrisation and non-dimensionalisation. This will set the grounds for the matched asymptotic expansion of the model in a limit where the processivity of the vesicles, respectively molecular motors is small (section 4). We perform the spectral analysis of the resulting limit problem (section 5) in order to single out the rate of convergence to steady state. Finally we discuss conclusions and implications in the last section.

2. Mathematical model

Secretory vesicles in the perinuclear, respectively subcortical region of chromaffin cells can be categorised as follows [14]: Vesicles are either diffusing freely, being caged or moving in a directed fashion. As a variation of this categorisation in the context of this study we will neglect the caged state and focus on the following three different groups of vesicles, 1) freely diffusing ones, 2) vesicles being bound - via a molecular motor protein - to a cytoskeleton fibre such that they undergo directed movement towards the periphery as well as 3) vesicles bound to a fibre in a way such that they move towards the centre of the cell.

The life-cycle we have in mind is depicted in figure 1: SVs are released into the cytoplasm at the Golgi apparatus. While some vesicles are diffusing freely in the cytoplasm, they might bind reversibly through linker proteins to larger protein clusters, especially cytoskeleton fibres or otherwise be restricted in motion. In [14] these vesicles were called caged, though we will neglect this population in the context of this study. Vesicles might also bind reversibly through cross-linker proteins to cytoskeleton fibres. We don't specify whether vesicles are bound to microtubules or F-actin and also not what kind of molecular motor is involved. We rather assume that binding is stochastic with given on- and off rates which possibly differ according to the direction of transport. Finally vesicles, reaching the cortex typically after alternating randomly between free diffusion and directed motion in either direction, would bind irreversibly to the cortex at a given rate which is when we - for the sake of this study - do not track them any more by excluding them from the three populations we model.

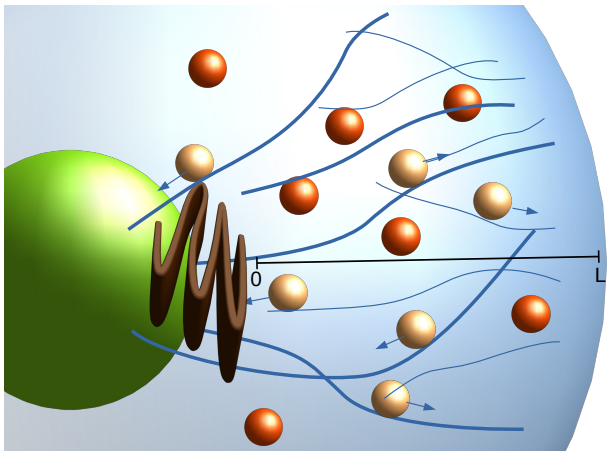

FIGURE 1. Sketch of the lifecycle of secretory vesicles as depicted by the mathematical model (1), (2) and (3): Between synthesis at the Golgi apparatus (brown) and irreversible binding to the cell cortex, SV might either float in the cytoplasm or be dragged through molecular motors along F-actin fibres (thin lines) and microtubules (thick lines).

Our goal is to formulate a system of PDEs which correspond to a mean field model for the spatial concentration of secretory vesicles in the cytoplasm. The spatial domain will be the interval $[0, L]$ where L is regarded as the distance - in the radial direction - between the location at $x = 0$ where newly synthesized vesicles are released into the cytoplasm and the cell cortex where secretory vesicles ultimately - we assume irreversibly - bind to the cortex and continue their trajectory through the cortex towards the site of exocytosis localized at the cellular membrane.

Obviously this neglects much of the spatial dynamics reducing motion to translocation in radial direction. We also neglect the spherical geometry of the cells and formulate the model without taking into account the distortion which would otherwise be introduced by the spherical coordinates.

The concentration of vesicles being transported towards the cortex is given by $f_+ = f_+(t, x)$ where $t \geq 0$ denotes time and $x \in [0, L]$ denotes the radial position. It satisfies

$$\begin{cases} \partial_t f_+ + a_+ f_+' = \kappa_+ c - \beta_+ f_+ \,, \\ f_+(0) = 0 \,, \end{cases} \tag{1}$$

where $a_+ > 0$ is the transport velocity. What we have in mind is that at their start these tracks are empty which accounts for the boundary condition in (1). Along the tracks vesicles which are freely moving in the cytoplasm - their concentration is given by $c = c(t, x)$ - bind to the fibers at the rate $\kappa_+ > 0$. In addition, bound vesicles also detach from the fibres and rejoin the pool of free vesicles at the rate $\beta_+ > 0$.

Alternatively freely moving vesicles might attach to fibres through molecular motor proteins which drag them towards the cell centre. This gives rise to an analogous model for their concentration $f_- = f_-(t, x)$ in which the speed of transport as well as on- and off-rates are given by $a_- > 0$, $\kappa_- > 0$ and $\beta_- > 0$. In this case, transport is from the cortex at $x = L$ towards the cell centre which accounts for the negative sign of the advection term and the boundary condition being imposed at $x = L$,

$$\begin{cases} \partial_t f_- - a_- f_-' = \kappa_- c - \beta_- f_- \,, \\ f_-(L) = 0 \,. \end{cases} \tag{2}$$

We remark that systems of equations such as (1), (2) arise in numerous biological applications, especially in the context of modelling the motion of molecular motors along single or bundle of microtubules [4, 17].

Finally the free vesicles which are undergoing random motion satisfy the reaction-diffusion equation

$$\begin{cases} \partial_t c = D_f c'' - (\kappa_+ + \kappa_-)c + \beta_+ f_+ + \beta_- f_- \,, \\ c(0) = \bar{c} \,, \\ D_f c'(L) = a_+ f_+(L) - \xi c(L) \,, \end{cases} \tag{3}$$

where $D_f > 0$ is the diffusion coefficient and the reaction terms correspond to the exchange terms described above. At the site of vesicle release at $x = 0$ the concentration is kept constant with value $\bar{c} > 0$ which mimics a fast feed-back mechanism by which the rate of vesicle synthesis is adjusted in a way such that their concentration is kept constant close to the Golgi apparatus. The boundary condition imposed at the cortex ($x = L$) describes the balance of diffusive flux of free vesicles, advection flux of fibre-bound vesicles and attachment of free vesicles to the cortex. We remark that the approach of modelling stimulation as an increased vesicle adsorption rate ξ at the cortex is motivated by the observed threefold increase of vesicle transitions from directed motion to caged, i.e. cytoskeleton bound, upon stimulation reported in [14]. Finally, assuming zero adsorption ($\xi = 0$) in control cells represents an idealisation of the residual secretion present in non-stimulated chromaffin cells.

Description	Symbol	Value	Reference
Concentration of chromaffin vesicles at Golgi apparatus	$\bar{c}$	$3000\ \mu m^{-1}$	Estimated with regard to figure 2D in [14].
Radial distance between Golgi apparatus and cortex	L	$5\,\mu m$	
Diffusion coefficient of free vesicles	D_f	$0.002\,\mu m^2 s^{-1}$	Figure S1 in [14].
Rate of fibre detachment	β_+, β_-	$0.02\,s^{-1}$	Estimated to reproduce the position of the concentration peak of vesicles undergoing directed motion [14].
Rate of fibre attachment	κ_+, κ_-	$0.0175\,s^{-1}$	Estimated relative to β in order to correctly predict the observed ratio of freely diffusing vs moving vesicles in [14].
Cortex binding velocity	ξ	$0.0\,\mu m\,s^{-1}$ (control), $0.03\,\mu m\,s^{-1}$ (stimulation)	Estimated
Transport speed	a_+, a_-	$0.04\,\mu m\,s^{-1}$	[14]

TABLE 1. List of parameter values

Numerical results for the steady state solutions using the parameter values listed in table 1 are shown in figure 2. These results indicate the presence of boundary layers at both ends of the domain. At $x = 0$ the concentrations of free vesicles and of vesicles being transported towards the cell centre exhibit peaks. At the right endpoint – corresponding to the region abutting the cortex – there are also concentration peaks, respectively a boundary layer which reflects the situation at $x = 0$. Upon stimulation the steady state profiles (figure 2 (right)) tilt towards the cortex where vesicles bind and start their further journey towards exocytosis.

The steady state concentrations in figure 2 (right) reproduce some of the key features of figure 2 (C and D) in [14]. In the perinuclear region the boundary layer with the pronounced peak in free vesicles at $x = 0$ corresponds to the large share of free vesicles found in the central region between 3 and 5 μm away from the cortex. The relative dominance of vesicles undergoing directed transport in the subcortical region of chromaffin cells corresponds to the relatively larger share of vesicles undergoing directed motion in figure 2 (blue curve). Finally, it can be observed that both the experimentally measured vesicle counts and the steady state concentrations of

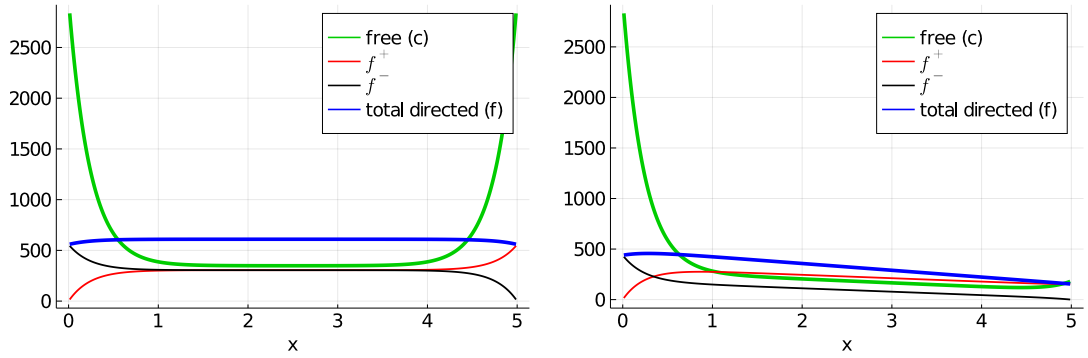

FIGURE 2. Steady state solutions for $\xi = 0$ (left) and for an activated cell ($\xi = 0.03$).

activated cells in our simulation display equally large shares of free and transported vesicles near the cortex.

	C	F^+	F^-	F^+/F^-	$(F^+ + F^-)/C$
control	2990	1524	1524	1.00	1.02
stimulation	1588	1083	536	2.02	1.02

TABLE 2. Total vesicle counts $C = \int_0^L c\,dx$, $F^+ = \int_0^L f^+\,dx$ and $F^- = \int_0^L f^-\,dx$, as well as ratios distal/proximal and free/directed at the steady states.

One of the prominent observations in [14] (figure 3S) was that upon stimulation the ratio of vesicles being transported towards the periphery vs towards the cell centre increases from about 1:1 to 2:1. As illustrated by the total vesicle counts listed in table 2 this shift could be exactly reproduced given a specific fit on the off-rates $\beta_\pm$. It should be noted that this fit also sets the on-rates $\kappa_\pm$ since the ratio of on- and off-rates determines the overall ratio of free vesicles vs. moving ones.

The study [14] also reports up-regulation of total directed transport upon stimulation. Indeed we found that when choosing some of parameter values for directed transport (on-rates $\kappa_\pm$, off-rates $\beta_\pm$ and transport speeds $a_\pm$) in a way such that they differed between distal and proximal transport, it was in principle possible to reproduce the overall up-regulation of directed transport.

However, from a modelling point of view it isn't clear which description of directional variation is appropriate. The associated parameter space (parameters ν, γ and b in the symmetrised model below) is higher-dimensional and needs to be further constrained. Therefore, in the context of the simulations in this study we assume equal rates. For these the ratio of total transport vs randomly moving cells does not change upon stimulation (see table 2).

Finally, we also remark that the absolute vesicle counts in figure 2D of the experimental study appear to increase linearly towards the cortex. This is due to the growth towards the periphery of the annular regions in which the vesicle counts were performed. In order to facilitate some of the explicit computations in the remaining part of this paper, this is neglected in the present study, i.e. we don't formulate the model with respect to spherical coordinates. Nevertheless, to gain further insight into the effect of directional variations, in the rest of this study we will focus on the derivation of a quasi-steady state approximation to the system (1), (2), (3).

3. SYMMETRISATION AND NON-DIMENSIONALISATION

We scale the system (1), (2), (3) using the reference values for spatial position, time and concentrations $x_c = L$, $t_c = L^2/D_f$ and $c_c = \bar{c} = f_c$. The scaled variables $\tilde{x} = x/L$, $\tilde{t} = t/t_c$ and

$\tilde{c} = c/\bar{c}$, $\tilde{f}_\pm = f_\pm/\bar{c}$ whose tildes we omit immediately satisfy

$$(4)\qquad \begin{cases} \partial_t c = c'' - (\kappa_+ + \kappa_-)c + \beta_+ f_+ + \beta_- f_- \ , \\ c(0) = 1 \ , \\ c'(1) = a_+ f_+(1) - \xi c(1) \ , \end{cases} \qquad \begin{cases} \partial_t f_\pm \pm a_\pm f_\pm' = \kappa_\pm c - \beta_\pm f_\pm \ , \\ f_+(0) = 0 = f_-(1) \ , \end{cases}$$

where the scaled versions of (1) and (2) are written into one single equation in which either the top symbols apply or the bottom ones. In this system the reaction rates $\beta_\pm$ and $\kappa_\pm$ are scaled by D_f/L^2, which is the inverse of the reference time, and the velocities $a_\pm$ and ξ by the reference speed $x_c/t_c = D_f/L$.

As a second step we introduce an alternative formulation of (4) based on symmetrised parameters. We introduce the total concentration of vesicles undergoing transport $f > 0$, their average speed $a > 0$, their combined attachment rate $\kappa > 0$ and their average unbinding rate $\beta > 0$. The respective differences are g, b, ν and γ.

$$\begin{array}{ll} f = f_+ + f_- & g = f_+ - f_- \\ a = (a_+ + a_-)/2 & b = (a_+ - a_-)/2 \\ \kappa = \kappa_+ + \kappa_- & \nu = \kappa_+ - \kappa_- \\ \beta = (\beta_+ + \beta_-)/2 & \gamma = (\beta_+ - \beta_-)/2 \end{array} \quad \text{which implies that} \quad \begin{array}{l} f_\pm = (f \pm g)/2 \\ a_\pm = a \pm b \\ \kappa_\pm = (\kappa \pm \nu)/2 \\ \beta_\pm = \beta \pm \gamma \end{array}$$

The resulting system is given by

$$(5)\qquad \begin{cases} \partial_t c = c'' - (\kappa c - \beta f) + \gamma g \ , \\ c(0) = 1 \ , \\ c'(1) = (a+b) f(1) - \xi c(1) \ , \end{cases} \qquad \begin{cases} \partial_t f + a g' + b f' = \kappa c - \beta f - \gamma g \ , \\ f(0) + g(0) = 0 \ , \end{cases} \qquad \begin{cases} \partial_t g + a f' + b g' = \nu c - \beta g - \gamma f \ , \\ g(1) = f(1) \ , \end{cases}$$

which is the starting point from where perform the matched asymptotic expansion.

4. Asymptotic expansion

In this section we will derive a new – and simpler – mathematical problem, the solutions of which will approximate solutions to the model (5) in the asymptotic regime, where the transitions of vesicles between directed motion and diffusive motion are fast, i.e. in which processivity is low.

We start by assuming that the average off-rate β and the joint on-rate κ scale like $1/\varepsilon^2$. To this end we interpret the dimensionless scaling parameter as $\varepsilon = \beta^{-1/2}$, i.e. we replace β by $1/\varepsilon^2$ (persistence), and we introduce the ratio of these rates $\alpha = \kappa/\beta$ (occupancy).

To obtain a meaningful limit model in the regime $\varepsilon \ll 1$ we found that a number of parameters should be of order $1/\varepsilon$, namely the average speed of transport a as well as the differential on- and off-rates γ and ν. The resulting modified system of equations is then given by

$$(6)\qquad \begin{cases} \partial_t c = c'' - \dfrac{1}{\varepsilon^2}(\alpha c - f) + \dfrac{1}{\varepsilon}\gamma g \ , \\ c(0) = 1 \ , \\ c'(1) = \left(\dfrac{1}{\varepsilon} a + b\right) f(1) - \xi c(1) \ , \end{cases} \qquad \begin{cases} \partial_t f + \dfrac{1}{\varepsilon} a g' + b f' = \dfrac{1}{\varepsilon^2}(\alpha c - f) - \dfrac{1}{\varepsilon}\gamma g \ , \\ f(0) + g(0) = 0 \ , \end{cases} \qquad \begin{cases} \partial_t g + \dfrac{1}{\varepsilon} a f' + b g' = \dfrac{1}{\varepsilon}\nu c - \dfrac{1}{\varepsilon^2}\beta g - \dfrac{1}{\varepsilon}\gamma f \ , \\ g(1) = f(1) \ . \end{cases}$$

Note that the steady state solutions shown in figure 2 indicate the presence of boundary layers at both ends of the interval. We address first the inner problem, namely finding an approximate solution to (6) which does not necessarily satisfy the boundary conditions. Indeed the inner problem which we obtain through straightforward asymptotic expansion is not fully determined, instead its boundary conditions will be determined by the solutions to the boundary layer problems.

Inner problem. The approximation of a solution to the inner problem is written as an expansion of c, f and g, namely $c \approx c_0 + \varepsilon c_1$, $f \approx f_0 + \varepsilon f_1 + \varepsilon^2 f_2$ and $g \approx g_0 + \varepsilon g_1 + \varepsilon^2 g_2$. The details of finding the leading order equations are in section A. We find that

$$f_i = \alpha c_i \ , \quad i = 0, 1 \ , \tag{7}$$

$$g_0 = 0 \ , \quad \text{and} \quad g_i = \nu c_{i-1} - \gamma \alpha c_{i-1} - a\alpha c'_{i-1} \quad \text{for} \quad i = 1, 2 \ , \tag{8}$$

as well as

$$\partial_t c_i + c'_i \frac{a\nu + \alpha(b - a\gamma)}{1 + \alpha} = \frac{1 + a^2\alpha}{1 + \alpha} c''_i \ , \quad i = 0, 1 \ . \tag{9}$$

Left boundary layer. For the asymptotic treatment of the left boundary layer we introduce the boundary layer variables $\bar{x} = x/\varepsilon$, $\bar{c}(t, \bar{x}) = c(t, \varepsilon\bar{x})$, $\bar{f}(t, \bar{x}) = f(t, \varepsilon\bar{x})$ and $\bar{g}(t, \bar{x}) = g(t, \varepsilon\bar{x})$. Applying these transformations in (6) we obtain the following boundary layer problem on $(0, \infty)$,

$$\begin{cases} \partial_t \bar{c} = \dfrac{1}{\varepsilon^2}\bar{c}'' - \dfrac{1}{\varepsilon^2}(\alpha\bar{c} - \bar{f}) + \dfrac{1}{\varepsilon}\gamma\bar{g} \ , \\ \partial_t \bar{f} + \dfrac{1}{\varepsilon^2} a\bar{g}' + \dfrac{1}{\varepsilon} b\bar{f}' = \dfrac{1}{\varepsilon^2}(\alpha\bar{c} - \bar{f}) - \dfrac{1}{\varepsilon}\gamma\bar{g} \ , \\ \partial_t \bar{g} + \dfrac{1}{\varepsilon^2} a\bar{f}' + \dfrac{1}{\varepsilon} b\bar{g}' = \dfrac{1}{\varepsilon}\nu\bar{c} - \dfrac{1}{\varepsilon^2}\bar{g} - \dfrac{1}{\varepsilon}\gamma\bar{f} \ , \end{cases} \tag{10}$$

coupled to the boundary conditions

$$\bar{c}(0) = 1 \ , \tag{11}$$

$$\bar{f}(0) + \bar{g}(0) = 0 \ . \tag{12}$$

We find the following approximation to leading order (for details see section B), $c \approx \bar{c}_0 + O(\varepsilon)$, $f \approx \bar{f}_0 + O(\varepsilon)$ and $g \approx \bar{g}_0 + O(\varepsilon)$, where

$$\bar{c}_0 = c_0(0) + (1 - c_0(0)) \exp\left(-\bar{x}\sqrt{\alpha + \frac{1}{a^2}}\right) \ ,$$

$$\bar{f}_0 = \alpha c_0(0) - \frac{1}{a^2}(1 - c_0(0)) \exp\left(-\bar{x}\sqrt{\alpha + \frac{1}{a^2}}\right) \ ,$$

$$\bar{g}_0 = \frac{-1}{a}(1 - c_0(0))\sqrt{\alpha + \frac{1}{a^2}} \exp\left(-\bar{x}\sqrt{\alpha + \frac{1}{a^2}}\right) \ ,$$

and

$$c_0(0) = \frac{1}{K} \quad \text{where} \quad K = \sqrt{\alpha a^2 + 1} \ . \tag{13}$$

Therefore the ratio between $\bar{c}_0(0)$ and the original boundary value $c(0) = 1$ is given by the constant K in (13).

Right boundary layer. To analyse the right boundary layer at $x = 1$ we introduce the boundary layer variables $\hat{x} = (x - 1)/\varepsilon + 1$ as well as $\hat{c}$, $\hat{f}$, $\hat{g}$ in the same way as above. Applying these transformations in (6) we obtain the right boundary layer problem (see appendix C). It couples the same equations as for the left boundary layer, namely (46) which is (10) written in terms of $\hat{c}(t, \hat{x})$, $\hat{f}(t, \hat{x})$, $\hat{g}(t, \hat{x})$, with the following boundary conditions,

$$\frac{1}{\varepsilon}\hat{c}'(1) = \left(\frac{1}{\varepsilon}a + b\right)\hat{f}(1) - \xi\hat{c}(1) \ , \tag{14}$$

$$\hat{f}(1) = \hat{g}(1) \ . \tag{15}$$

The leading order approximation $\hat{c} \approx \hat{c}_0 + o(\varepsilon)$, $\hat{f} \approx \hat{f}_0 + o(\varepsilon)$, $\hat{g} \approx \hat{g}_0 + o(\varepsilon)$ satisfies the following system of equations which we obtain by equating the leading order terms in (46), (14), (15),

namely

$$\begin{cases} 0 = \hat{c}_0'' - (\alpha\hat{c}_0 - \hat{f}_0) \ , \\ a\hat{g}_0' = (\alpha\hat{c}_0 - \hat{f}_0) \ , \\ a\hat{f}_0' = -\hat{g}_0 \ , \end{cases} \tag{16}$$

with boundary conditions

$$\hat{f}_0(1) - \hat{g}_0(1) = 0 \ , \tag{17}$$

$$\hat{c}_0'(1) = a\hat{f}_0(1) \ . \tag{18}$$

Again it is our primary goal to determine concentrations in the far field $\hat{x} \to -\infty$ and to match them with the inner solution $c_0(1)$, $f_0(1)$ and $g_0(1)$. Given a general solution of the system of equations (16) the first boundary condition implies the ratio

$$\hat{c}_0(1) = Kc_0(1) \tag{19}$$

with the same constant of proportionality (13) as for the left boundary layer (see appendix C).

Interestingly the two boundary conditions (17) and (18) are redundant and one may derive the same result evaluating (18) for the general solution of (16). The reason is that in (18) attachment to the cortex with rate ξ is neglected in the limit as $\varepsilon \to 0$ and therefore the respective term isn't present in (18). As a consequence both boundary conditions (17) and (18) model the same pathway, namely that all vesicles which arrive at the cortex by directed transport enter the pool of free vesicles. This is the immediate interpretation of (18) but it is also implied by (17) which states that no vesicles leave the cortex at $x = 1$ through direct transport towards the nucleus. For a detailed derivation of (19) in both cases see appendix C. We obtain the following solution to the right boundary layer problem,

$$\hat{c}_0 = c_0(1)\left(1 + (K-1)\exp\left((\hat{x}-1)\sqrt{\alpha + \frac{1}{a^2}}\right)\right) \ , \tag{20}$$

$$\hat{f}_0 = c_0(1)\left(\alpha - \frac{K-1}{a^2}\exp\left((\hat{x}-1)\sqrt{\alpha + \frac{1}{a^2}}\right)\right) \ , \tag{21}$$

$$\hat{g}_0 = c_0(1)\sqrt{\alpha + \frac{1}{a^2}}\,\frac{K-1}{a}\exp\left((\hat{x}-1)\sqrt{\alpha + \frac{1}{a^2}}\right) \ , \tag{22}$$

with the same constant K as identified in (13).

4.1. **Limit problem.** Now we assemble the identities found above to obtain a system of equations which approximates (6) uniformly in the limit as $\varepsilon \to 0$.

The leading order term of the expansion of solutions to the inner problem satisfies (9), i.e.

$$\partial_t c_0 + Vc_0' = Dc_0'' \ , \tag{23}$$

where we have introduced the following short notation for the effective drift and diffusion,

$$V := \frac{a\nu + \alpha(b - a\gamma)}{1+\alpha} \quad \text{and} \quad D := \frac{1 + a^2\alpha}{1+\alpha} \ .$$

The left boundary condition is given by (13) according to the solution of the left boundary layer problem. The leading order solution of the right boundary layer problem suggests that the same ratio (19) is assumed by $c_0(1)$ and the "actual right boundary value of $c(1)$" which is therefore given by $Kc_0(1)$. However, this insight doesn't provide a boundary condition to complement (23). It appears that one piece of information is missing. Indeed so far we've neglected the fact that even in the regime where ε is very small numerical simulations of the full model (6) such as those shown in figure 2 indicate that adsorbtion at the cortex with rate ξ doesn't become zero.

This indicates that we've neglected the adsorption flux at $x = 1$ so far. In the limit $\varepsilon \to 0$, however, the "width" of the boundary layer vanishes and so the flux at the right boundary of

the inner problem must equal the adsorption flux $\xi K c_0(1)$. This provides the missing piece of information and as a consequence the resulting system of equations satisfied by c_0 – the fully determined inner problem – is given by

$$\begin{cases} \partial_t c_0 + V c_0' = D c_0'' \,, \\ c_0(0) = \dfrac{1}{K} \,, \\ -D c_0'(1) + V c_0(1) = \dfrac{\xi K}{1+\alpha} c_0(1) \,, \end{cases} \tag{24}$$

where the last equation represents the equality of fluxes at the right endpoint. Note that we need to take the flux with respect to the entire vesicle population which explains the factor $1/(1+\alpha)$.

As a consequence of (7) and (8) the other leading order terms in the asymptotic expansions of c and f are given by

$$f \approx f_0 \,, \quad \text{where} \quad f_0 = \alpha c_0 \tag{25}$$

and

$$g \approx \varepsilon g_1 = \varepsilon(\nu c_0 - \gamma f_0 - a f_0') = \varepsilon((\nu - \gamma\alpha) c_0 - a\alpha c_0') \,. \tag{26}$$

The matched asymptotic expansion – up to leading order – of the system of diffusion and advection equations (6) is therefore given by

$$\begin{aligned} c_{\text{appr}} &= c_0 + \bar{c}_0\left(\frac{x}{\varepsilon}\right) + \hat{c}_0\left(\frac{x-1}{\varepsilon} + 1\right) - \frac{1}{K} - c_0(1) \\ &= c_0 + (1 - c_0(0)) \exp\left(-\frac{x}{\varepsilon}\sqrt{\alpha + \frac{1}{a^2}}\right) + c(1)\left((K-1)\exp\left(-\frac{1-x}{\varepsilon}\sqrt{\alpha + \frac{1}{a^2}}\right)\right) \,, \end{aligned} \tag{27}$$

where, following the standard approach for matching boundary layer solutions and inner solution (see e.g. [11]), we have subtracted the "common" part of the inner and boundary layer solutions at both endpoints of the interval.

The quality of the uniform approximation is illustrated by figure 3 which compares the steady state solution of the system (1), (2), (3) (specifically its dimensionless version (6)) to the steady state solution c_0 of the inner problem (24) and to the uniform approximation c_{appr} given in (27). For the set of parameters which corresponds to table 1 a small deviation at the right endpoint which determines the adhesion flux at the cortex is noticeable. For an even smaller value of the scaling parameter ε this discrepancy vanishes which illustrates the uniform convergence of the leading order term c_{appr} in the matched asymptotic expansion.

5. Steady state and spectral analysis

In this section we will perform the spectral analysis of the approximating system (24). It is our goal to identify the time-scale during which the system adapts to the variation of vesicle binding affinity ξ upon stimulation.

At the steady state written as $c_{0,\infty}(x)$, the system (24) implies that

$$V c_{0,\infty} - D c_{0,\infty}' \equiv J \,, \tag{28}$$

where, for the time being, we use the notation $J := \xi K c_{0,\infty}(1)/(1+\alpha)$ to hide the fact that the flux is coupled linearly to the right boundary value of $c_{0,\infty}$. Multiplying by the integrating factor $\exp(-xV/D)$ allows us to write (28) as $J \exp\left(-\frac{V}{D}x\right) = -D\left(c_{0,\infty}\exp\left(-\frac{V}{D}x\right)\right)'$. Integrating on $(0,x)$ we find that

$$c_{0,\infty}(x) = \frac{1}{K}\exp\left(\frac{V}{D}x\right) - \left(\exp\left(\frac{V}{D}x\right) - 1\right)\frac{J}{V} \,, \tag{29}$$

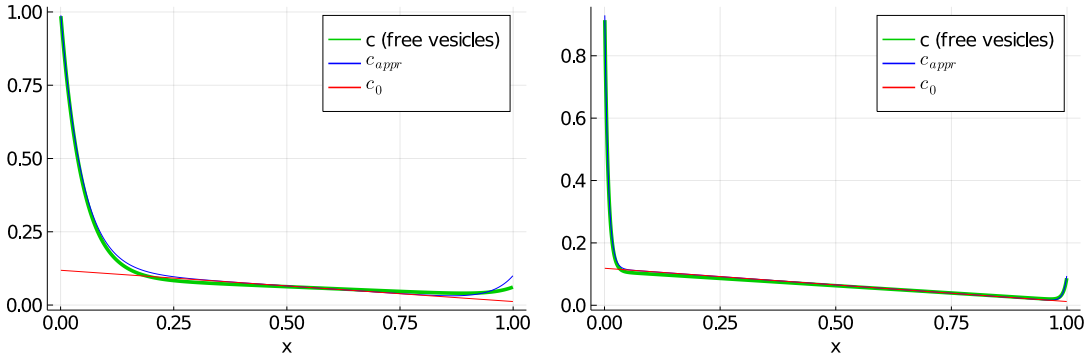

FIGURE 3. Steady state solution c of the system (6) for an activated cell and the corresponding solution of the asymptotic model (24) c_0 as well as the uniform approximation c_{appr}, which includes the boundary layers. Left: The parameters are the dimensionless versions of those listed in table 1 which involves$\varepsilon \approx 0.06$. Right: For a smaller scaling parameter, $\varepsilon = 0.01$, the steady state solutions coincide very closely which illustrates the convergence to the asymptotic limit.

where we used the boundary condition in (24). To determine the flux J we evaluate at $x = 1$ and obtain the Michaelis-Menten-type law

$$J = \frac{\xi K}{1+\alpha} c_{0,\infty}(1) = \xi \frac{\exp\left(\frac{V}{D}\right)}{\left(1+\alpha+\left(\exp\left(\frac{V}{D}\right)-1\right)\frac{\xi K}{V}\right)} = V_{\max}\frac{\xi}{K_m+\xi}\ , \tag{30}$$

where $V_{\max} = \frac{V}{K}\frac{1}{1-e^{-V/D}}$ and $K_m = \frac{1+\alpha}{\exp(\frac{V}{D})-1}\frac{V}{K}$. Note that in the asymptotic regime where the effective drift V is small it holds that $V_{\max} \approx \frac{D}{K} + \frac{V}{2K}$ and $K_m \approx (1+\alpha)(\frac{D}{K} - \frac{V}{2K})$. In the limit where $V \to 0$ the concentration profile (29) reduces to

$$c_{0,\infty}(x) = 1/K - xJ/D = 1/K - x\xi\frac{1}{(1+\alpha)D + K\xi}\ .$$

Linearising the model (24) in this case simply requires to use absorbing boundary condition at the left endpoint. The resulting system for the perturbation δc_0,

$$\begin{cases} \lambda\delta c_0 = D\,\delta c_0'' - V\,\delta c_0'\ , \\ \delta c_0(0) = 0\ , \\ -D\,\delta c_0'(1) + (V - \xi K/(1+\alpha))\,\delta c_0(1) = 0\ , \end{cases} \tag{31}$$

can be written as Sturm-Liouville eigenvalue problem $\lambda\delta c_0 = D\exp\left(\frac{V}{D}x\right)\left(\delta c_0'\exp\left(-\frac{V}{D}x\right)\right)'$, which implies that there is a countable sequence of real eigenvalues $\lambda_1 > \lambda_2 > \dots$. To solve this eigenvalue problem we consider a solution of the system

$$\begin{cases} \bar\lambda\delta c = \delta c'' - \bar V\,\delta c'\ , \\ -\delta c'(1) + (\bar V - \bar\xi)\,\delta c(1) = 0\ , \end{cases}$$

where $\bar\lambda = \lambda/D$ and $\bar V = V/D$ as well as $\bar\xi = \xi K/(D(1+\alpha))$ which simplifies to $\bar\xi = \xi/K$. Its solution is given by

$$\delta c = e^{-\frac{1}{2}x(\sqrt{u}-\bar V)}\left(\left(2\bar\xi - \bar V + \sqrt{u}\right) + \left(-2\bar\xi + \bar V + \sqrt{u}\right)e^{\sqrt{u}(x-1)}\right)\ ,$$

where $u = 4\bar\lambda + \bar V^2$. Eigenfunctions satisfy the vanishing boundary condition in (31), $\delta c(0) = 0$, i.e. $0 = (v+\sqrt{u}) + (-v+\sqrt{u})\,e^{-\sqrt{u}}$ where $v = 2\bar\xi - \bar V$. We introduce the function $f(u) :=$

$-\sqrt{u}\coth\left(\frac{\sqrt{u}}{2}\right)$ which allows to write this equation as $v = f(u)$. Note that

$$f(u) = \begin{cases} -\sqrt{u}\coth\left(\frac{\sqrt{u}}{2}\right) & u > 0\,, \\ -2 & u = 0\,, \\ -\sqrt{-u}\cot\left(\frac{\sqrt{-u}}{2}\right) & u < 0\,. \end{cases} \tag{32}$$

Since this function can be written in terms of the cot-function when $u < 0$ the function f has singularities located at $u = -4\pi^2k^2$, $k = 1, 2, ...$ (see figure 4 (left)).

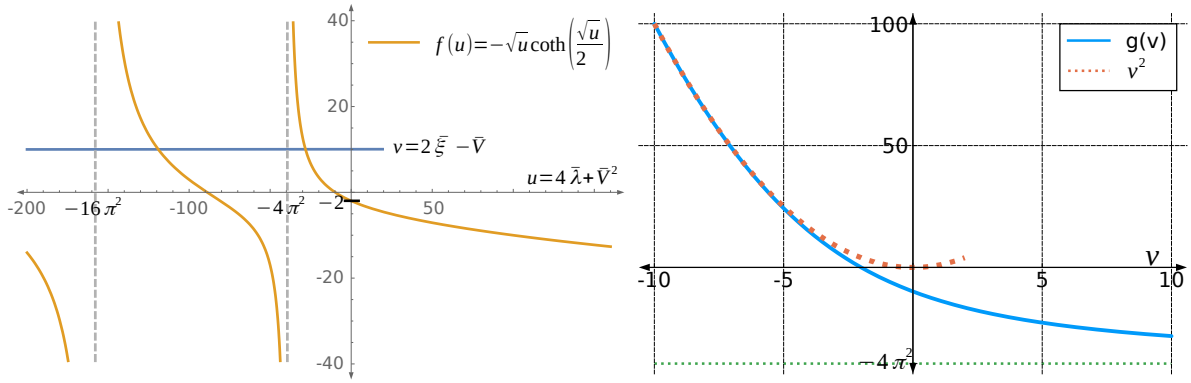

FIGURE 4

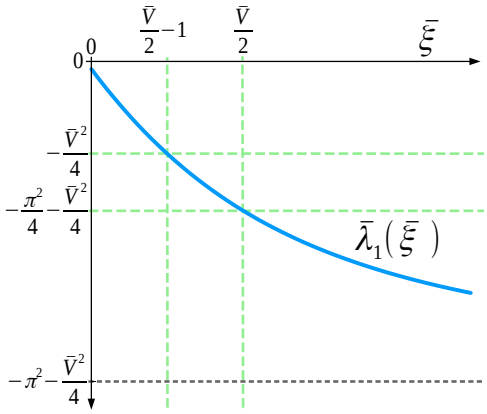

FIGURE 5. $\bar{\lambda}_1$ as a function of $\bar{\xi}$ (here for $\bar{V} > 2$).

To identify the leading eigenvalue λ_1 which determines the rate at which the system approaches equilibrium we also introduce the function g as the inverse of the first, i.e. rightmost, branch of f, i.e. $g : (-4\pi^2, \infty) \mapsto \mathbb{R}$. Its graph is shown in figure 4 (right). Then for the leading eigenvalue it holds that $v = 2\bar{\xi} - \bar{V} = f(4\bar{\lambda}_1 + \bar{V}^2)$, i.e.

$$\bar{\lambda}_1 = \frac{1}{4}\left(g(2\bar{\xi} - \bar{V}) - \bar{V}^2\right)\,,$$

which is sketched in figure 5. Note that this implies lower and upper bounds. Since $\bar{\xi} > 0$ and since g is monotonically decaying, satisfying $g(v) < v^2$, we obtain $\bar{\lambda}_1 < \frac{1}{4}(g(-\bar{V}) - \bar{V}^2) < 0$ as well as $\bar{\lambda}_1 < \frac{1}{4}((2\bar{\xi} - \bar{V})^2 - \bar{V}^2) = \bar{\xi}(\bar{\xi} - \bar{V})$. In addition, since $g(v) > -4\pi^2$ we also find that $\bar{\lambda}_1 > \frac{1}{4}(-4\pi^2 - \bar{V}^2) = -\pi^2 - \bar{V}^2/4$. Summarising, we obtain the following inequality for the leading eigenvalue,

$$-\pi^2 - \frac{\bar{V}^2}{4} < \bar{\lambda}_1 < \min\left(0, \bar{\xi}(\bar{\xi} - \bar{V})\right)\,,$$

which is reflected in the sketch of $\bar{\lambda}_1$ as a function of $\bar{\xi}$ in figure 5. Note that the following explicit function values of g, $g(0) = -\pi^2$ and $g(-2) = 0$, imply closed-form expressions for the

associated function values of $\bar{\lambda}_1$ which are highlighted in figure 5 as intersections of the green, dashed lines.

6. Discussion

In this study we model the conveyor belt mechanism for the replenishing of secretory vesicles proposed in [14], i.e. the concept that directional transport towards the periphery of the cell replenishes the pool of releasable secretory vesicles upon stimulation. Our goal has been to confirm the effectiveness of the proposed mechanism by a quantitative model and to answer the question whether mechano-chemical feedback mechanisms are required to sustain the observed adaption of transport characteristics upon stimulation. This involves up-regulation of transport directionality towards the cell periphery as well as up-regulation of total directed transport.

The model we suggest is a system of partial differential equations in one dimension which involves a reaction-diffusion equation for free vesicles as well as advection equations for the pools of vesicles undergoing directed motion in either direction. For an appropriate set of parameters we compute the steady state distributions in control and upon stimulation, which in our model is assumed to effectuate accelerated binding of vesicles to the cortex from where they continue their pathway towards exocytosis.

To better understand the characteristics of the mathematical solution of this model and how it is affected by the parameters we use matched asymptotic expansion to find a quasi-steady state approximation in the limit of low persistence of vesicle transport. The result is a drift-diffusion equation with effective drift and diffusivity for the leading term in the inner expansion as well as correction terms at the two boundaries of the domain. They describe the profile of the two boundary layers which are equally present in the solutions of the original model, though we remark that boundary layers are not visible in the vesicle count histograms in [14]. They are rather a modelling artefact since we concentrate synthesis at the Golgi-apparatus and caging at the cortex to respective boundary points of the 1D domain whereas in the living cell these phenomena are effective within a wider region.

Using the asymptotic limit model we compute the Michaelis-Menten-type law (30) for the adhesion flux of secretory vesicles at the cortex.

An important finding derived from the asymptotic expansion is that even though the rates for vesicle binding, unbinding and their speed of transport might differ between forward and backward transport, according to (25) the ratio of total transported vs freely diffusing vesicles is not affected by stimulation up to first order with respect to the scaling parameter representing persistence. Furthermore from (26) we infer that when we omit persistence of cargo transport, then even in stimulated cells transport is not directional, i.e. has no preferred direction. This underlines the importance of the role that the persistence of cargo transport plays for the conveyor belt mechanism. Unfortunately this also means that the impact of omitting persistence has to be weighted into the predictions of the asymptotic model for the conveyor belt mechanism.

Finally we compute the (exponential) rate at which the asymptotic model converges to steady state. It predicts the timescale within which the conveyor-belt mechanism adapts to stimulation. For the parameter values used in this study the relevant timescales in physical units ($t_c\lambda_1^{-1}$) are 196 sec (control) and 60.3 sec (stimulation). The resulting prediction, which is amenable to experimental testing, is that the system adapts significantly faster to stimulation than to omitting the stimulus.

We reiterate that the simulations indeed reproduce many of the experimental observations and this confirms the effectiveness of the conveyor belt mechanism. We notice especially that the up-regulation of directionality towards the periphery is correctly predicted by the model. The underlying mechanism is illustrated by the leading order term in the asymptotic expansion (26) and requires persistence, i.e $\varepsilon = \beta^{-1/2} > 0$. From this term it becomes clear that the directional-dependence of attachment and detachment rates (ν, γ) leads to a directional bias.

Yet even without such in-homogeneity between forward and backward transport we observe up-regulation of directionality upon stimulation. This effect is reflected by the term $a\alpha c_0'$ in (26) and relies on the concentration gradient of free vesicles after stimulation. Loosely speaking, given that vesicles in our model remain attached to a specific fibre, undergoing transport for

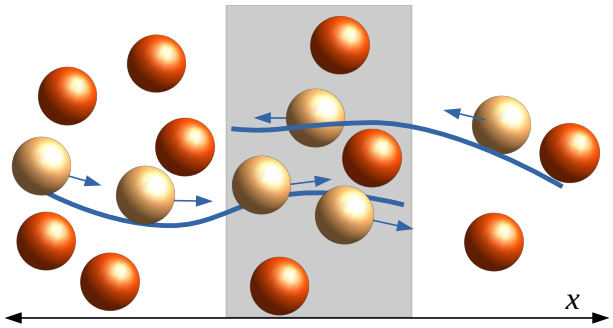

FIGURE 6. Directionality of transport through persistence and free vesicle concentration gradient.

an average distance given by a/β – this is the essence of persistence – differences in free vesicle concentration occuring within regions of this size have the following impact sketched in figure 6: looking at a specific region between the cell centre and the periphery (here in grey) the number of vesicles moving into this region coming from the cell centre is proportional to the number of free vesicles in the region preceding it - here on the left. The number of vesicles in the same region moving in the opposite direction is also approximately proportional to the number of free vesicles in the preceding region, which for these vesicles is located on the right. The difference of free vesicle concentrations between the regions left and right therefore translates into a direction-dependent concentration difference among the vesicles undergoing cargo transport within the grey region. Note that this is reflected in the steady state under stimulation visualised in figure 2. In this scenario the free vesicle concentration gradient is mostly constant and so is the difference between the two concentrations of vesicles undergoing transport in figure 2 (blue and red curve).

The other central phenomenon reported in [14] is up-regulation of total directed transport upon stimulation. We note that the modelling paradigm chosen in this study is probably not of the right degree of detail to address this question as the range of parameters which would allow an explanation of this phenomenon appears to be under-determined. The asymptotic limit model shows that the underlying mechanism certainly relies on persistence as illustrated by (25) according to which the ratio of total transport vs free diffusion is not affected by stimulation up to the first order with respect to the scaling parameter representing persistence. We therefore postpone a detailed analysis of the conditions that facilitate the up-regulation of transport to a future study in which we will employ a different modelling paradigm specifically targeting this phenomenon.

APPENDIX A. INNER PROBLEM

Equating terms of equal order in (6) we find the following equations relating terms in the expansions of c, f and g.

$O\left(\varepsilon^{-2}\right)$: We find that

$$f_0 = \alpha c_0 \,, \tag{33}$$

$$g_0 = 0 \,, \tag{34}$$

i.e. the ratio of the leading order terms, free vesicles vs. transported vesicles, is fixed and at the leading order the differential term vanishes.

$O\left(\varepsilon^{-1}\right)$: Equating terms of order ε^{-1}, the differential term at first order is given by

$$g_1 = \nu c_0 - \gamma f_0 - a f_0' \,, \tag{35}$$

and the ratio of free vesicles vs. transported ones is given by α even at first order since

$$\alpha c_1 - f_1 = a g_0' = 0 \,, \tag{36}$$

where we used (34).

$O(1)$: From the first two systems in (6) we obtain

$$\partial_t c_0 = c_0'' - (\alpha c_2 - f_2) + \gamma g_1 \,, \tag{37}$$

$$\partial_t f_0 + a g_1' + b f_0' = (\alpha c_2 - f_2) - \gamma g_1 \,, \tag{38}$$

which implies, taking the sum and using (33) and (35), that

$$\partial_t c_0 + c_0' \frac{a\nu + \alpha(b - a\gamma)}{1+\alpha} = \frac{1 + a^2\alpha}{1+\alpha} c_0'' \,.$$

From the third system in (6) we obtain

$$g_2 = \nu c_1 - \gamma f_1 - a f_1' \,, \tag{39}$$

where we used (34).

$O(\varepsilon)$: Likewise, taking the sum of the $O(\varepsilon)$ terms in the equations for c and f in (6) and using (36) and (39) we obtain

$$\partial_t c_1 + c_1' \frac{a\nu + \alpha(b - a\gamma)}{1+\alpha} = \frac{1 + a^2\alpha}{1+\alpha} c_1'' \,. \tag{40}$$

Appendix B. Left boundary layer

We focus on an expansion up to leading order only, i.e. $c \approx \bar{c}_0 + O(\varepsilon)$, $f \approx \bar{f}_0 + O(\varepsilon)$ and $g \approx \bar{g}_0 + O(\varepsilon)$, and obtain

$$0 = \bar{c}_0'' - (\alpha \bar{c}_0 - \bar{f}_0) \,, \tag{41}$$

$$a \bar{g}_0' = (\alpha \bar{c}_0 - \bar{f}_0) \,, \tag{42}$$

$$a \bar{f}_0' = -\bar{g}_0 \tag{43}$$

with boundary conditions

$$\bar{f}_0(0) + \bar{g}_0(0) = 0 \,, \tag{44}$$

$$\bar{c}_0(0) = 1 \,. \tag{45}$$

Taking a derivative of (43) and coupling with (42) and (41) respectively, we find that $-a^2 \bar{f}_0'' = a\bar{g}_0' = \alpha \bar{c}_0 - \bar{f}_0 = \bar{c}_0''$. Hence $-a^2 \bar{f}_0 = \bar{c}_0 + Ax + B$ for two constants A and B. Since in the far field ($\tilde{x} \to \infty$) we expect that the following matching conditions hold, $\bar{c}_0 \to c_0(0)$ and, as a consequence of (33), $\bar{f}_0 \to \alpha c_0(0)$ we obtain $A = 0$ and $-a^2 \alpha c_0(0) = c_0(0) + B$, i.e. $B = -c_0(0)(1 + \alpha a^2)$.

From this we conclude $\bar{f}_0 = \frac{-1}{a^2}\left(\bar{c}_0 - c_0(0)(1 + \alpha a^2)\right)$ which we substitute in (41) to obtain an equation for $\bar{c}_0$,

$$\begin{aligned} \bar{c}_0'' &= \alpha \bar{c}_0 - \bar{f}_0 \\ &= \alpha \bar{c}_0 + \frac{1}{a^2}\left(\bar{c}_0 - c_0(0)(1 \alpha a^2)\right) \\ &= (\bar{c}_0 - c_0(0)) \left(\alpha + \frac{1}{a^2}\right) \,. \end{aligned}$$

Coupling this with (45) we obtain

$$\bar{c}_0 = c_0(0) + (1 - c_0(0)) \exp\left(-x\sqrt{\alpha + \frac{1}{a^2}}\right) \,,$$

$$\begin{aligned}\bar{f}_0 &= \frac{-1}{a^2}\left(\bar{c}_0 - c_0(0)(1+\alpha a^2)\right)\\ &= \frac{-1}{a^2}\left(\bar{c}_0 - c_0(0) - \alpha a^2 c_0(0)\right)\\ &= \frac{-1}{a^2}\left((1-c_0(0))\exp\left(-x\sqrt{\alpha+\frac{1}{a^2}}\right) - \alpha a^2 c_0(0)\right)\\ &= \frac{-1}{a^2}(1-c_0(0))\exp\left(-x\sqrt{\alpha+\frac{1}{a^2}}\right) + \alpha c_0(0)\ ,\end{aligned}$$

and

$$\begin{aligned}\bar{g}_0 = -a\bar{f}_0' &= -a\left(\frac{-1}{a^2}(1-c_0(0))\exp\left(-x\sqrt{\alpha+\frac{1}{a^2}}\right) + \alpha c_0(0)\right)'\\ &= -a\left(\frac{1}{a^2}(1-c_0(0))\sqrt{\alpha+\frac{1}{a^2}}\exp\left(-x\sqrt{\alpha+\frac{1}{a^2}}\right)\right)\\ &= \frac{-1}{a}(1-c_0(0))\sqrt{\alpha+\frac{1}{a^2}}\exp\left(-x\sqrt{\alpha+\frac{1}{a^2}}\right)\ .\end{aligned}$$

We determine the far field $c_0(0)$ so that (44) is satisfied, i.e. $0 = (1-c_0(0)) - c_0(0)\alpha a^2 + (1-c_0(0))\sqrt{\alpha a^2+1}$ and conclude that

$$c_0(0) = \frac{1+\sqrt{\alpha a^2+1}}{1+\alpha a^2+\sqrt{\alpha a^2+1}} = \frac{1+\sqrt{\alpha a^2+1}}{(1+\sqrt{\alpha a^2+1})\sqrt{\alpha a^2+1}} = \frac{1}{\sqrt{\alpha a^2+1}} = \frac{1}{K}\ ,$$

where K is defined in (13) and represents the ratio between $c_0(0)$ and the actual boundary value $\bar{c}_0(0)$.

Appendix C. Right boundary layer

The system (6) written with respect to the right boundary layer variables $\hat{c}$, $\hat{f}$, $\hat{g}$ and $\hat{x}$, reads

$$\begin{cases}\partial_t\hat{c} = \dfrac{1}{\varepsilon^2}\hat{c}'' - \dfrac{1}{\varepsilon^2}(\alpha\hat{c}-\hat{f}) + \dfrac{1}{\varepsilon}\gamma\hat{g}\ ,\\ \partial_t\hat{f} + \dfrac{1}{\varepsilon^2}a\hat{g}' + \dfrac{1}{\varepsilon}b\hat{f}' = \dfrac{1}{\varepsilon^2}(\alpha\hat{c}-\hat{f}) - \dfrac{1}{\varepsilon}\gamma\hat{g}\ ,\\ \partial_t\hat{g} + \dfrac{1}{\varepsilon^2}a\hat{f}' + \dfrac{1}{\varepsilon}b\hat{g}' = \dfrac{1}{\varepsilon}\nu\hat{c} - \dfrac{1}{\varepsilon^2}\hat{g} - \dfrac{1}{\varepsilon}\gamma\hat{f}\ ,\end{cases} \tag{46}$$

coupled to the boundary conditions

$$\frac{1}{\varepsilon}\hat{c}'(1) = \left(\frac{1}{\varepsilon}a+b\right)\hat{f}(1) - \xi\hat{c}(1)\ , \tag{47}$$

$$\hat{f}(1) = \hat{g}(1)\ . \tag{48}$$

The leading order terms in the expansion $\hat{c}\approx\hat{c}_0+O(\varepsilon)$, $\hat{f}\approx\hat{f}_0+O(\varepsilon)$ and $\hat{g}\approx\hat{g}_0+O(\varepsilon)$ satisfy the system of equations

$$0 = \hat{c}_0'' - (\alpha\hat{c}_0 - \hat{f}_0)\ , \tag{49}$$

$$a\hat{g}_0' = (\alpha\hat{c}_0 - \hat{f}_0)\ , \tag{50}$$

$$a\hat{f}_0' = -\hat{g}_0\ , \tag{51}$$

as well as the boundary conditions

$$\hat{f}_0(1) = \hat{g}_0(1)\ , \tag{52}$$

$$\hat{c}_0'(1) = a\hat{f}_0(1)\ . \tag{53}$$

Using equations (51), (50) and (49) we obtain $-a^2\hat{f}_0'' = a\hat{g}_0' = \alpha\hat{c}_0 - \hat{f}_0 = \hat{c}_0''$. Hence, for two arbitrary constants A and B it holds that $-a^2\hat{f}_0 = \hat{c}_0 + Ax + B$. It is our goal to match the solution of the right boundary layer problem to the solution to the inner problem, therefore we expect that in the far field $\hat{x} \to -\infty$ it holds that $\hat{f}_0 = f_0(1) = \alpha c_0(1)$ where we used (33). Therefore we find that $A = 0$ and $B = -c_0(1)(1+\alpha a^2)$. As a consequence it holds that

$$\hat{f}_0 = \frac{-1}{a^2}\left(\hat{c}_0 - c_0(1)(1+\alpha a^2)\right) , \tag{54}$$

which we substitute in (49) to obtain

$$\begin{aligned}\hat{c}_0'' &= \alpha\hat{c}_0 + \frac{1}{a^2}\left(\hat{c}_0 - c_0(1)(1+\alpha a^2)\right)\\ &= \alpha\hat{c}_0 + \frac{1}{a^2}\left(\hat{c}_0 - c_0(1)\right) - \alpha c_0(1)\\ &= \left(\hat{c}_0 - c_0(1)\right)\left(\alpha + \frac{1}{a^2}\right) .\end{aligned}$$

Coupling this to the matching condition $\lim_{\hat{x}\to-\infty}\hat{c}_0(\hat{x}) = c_0(1)$ we obtain

$$\hat{c}_0 = c_0(1)\left(1 + (\hat{K}-1)\exp\left((\hat{x}-1)\sqrt{\alpha+\frac{1}{a^2}}\right)\right) \tag{55}$$

for a constant $\hat{K}$. Substituting (55) in (54) we also find

$$\hat{f}_0 = c_0(1)\left(\alpha - \frac{\hat{K}-1}{a^2}\exp\left((\hat{x}-1)\sqrt{\alpha+\frac{1}{a^2}}\right)\right) . \tag{56}$$

The constant $\hat{K}$ can be determined by coupling these results to either (52) or (53). Substituting (55) and (56) in (53) we find that

$$\begin{aligned}0 &= c_0(1)(\hat{K}-1)\sqrt{\alpha+\frac{1}{a^2}} - ac_0(1)\left(\alpha - \frac{\hat{K}-1}{a^2}\right)\\ &= c_0(1)\left((\hat{K}-1)\left(\sqrt{\alpha+\frac{1}{a^2}} + \frac{1}{a}\right) - \alpha a\right)\end{aligned}$$

which implies

$$\hat{K} = \frac{\alpha a}{\sqrt{\alpha+\frac{1}{a^2}}+\frac{1}{a}} + 1 = \frac{\alpha a^2}{\sqrt{\alpha a^2+1}+1} + 1 = \frac{\alpha a^2 + \sqrt{\alpha a^2+1}+1}{\sqrt{\alpha a^2+1}+1} = \sqrt{\alpha a^2+1} \tag{57}$$

which equals the constant of proportionality K we found before for the left boundary layer. Note that coupling (55), (54) with (52) instead leads to the same result according to computations which mimic those to find K in the left boundary layer: First substitute (56) in (51) to find

$$\hat{g}_0 = -a\hat{f}_0' = c_0(1)\sqrt{\alpha+\frac{1}{a^2}}\frac{\hat{K}-1}{a}\exp\left((\hat{x}-1)\sqrt{\alpha+\frac{1}{a^2}}\right) ,$$

which, together with (56), we substitute in (52) to obtain

$$0 = c_0(1)\left(\alpha - \frac{\hat{K}-1}{a^2}\right) - c_0(1)\sqrt{\alpha+\frac{1}{a^2}}\frac{\hat{K}-1}{a} ,$$

which leads to (57).

Acknowledgement

The author wants is thankful for valuable discussions with Calvin Zhang (U. of Arizona) and Elaine Schenk (UQ).

DO was supported by ARC Discovery Project DP180102956.

References

[1] Patricia Ñeco, Daniel Giner, María Del Mar Francés, Salvador Viniegra., and Luis M. Gutiérrez. Differential participation of actin- and tubulin-based vesicle transport systems during secretion in bovine chromaffin cells. *European Journal of Neuroscience*, 18(4):733–742, 2003.

[2] Kari Barlan and Vladimir I. Gelfand. Microtubule-based transport and the distribution, tethering, and organization of organelles. *Cold Spring Harbor Perspectives in Biology*, 9(5), 2017.

[3] M Birbaumer and F Schweitzer. Agent-based modeling of intracellular transport. *The European Physical Journal B*, 82(245), 2011.

[4] Paul C Bressloff. *Stochastic processes in cell biology*, volume 41. Springer, 2014.

[5] Susan S. Brown. Cooperation between microtubule- and actin-based motor proteins. *Annual Review of Cell and Developmental Biology*, 15(1):63–80, 1999. PMID: 10611957.

[6] Juliane P. Caviston and Erika L.F. Holzbaur. Microtubule motors at the intersection of trafficking and transport. *Trends in Cell Biology*, 16(10):530 – 537, 2006. Membrane Dynamics.

[7] Wenhai Chen, Wen Zhou, Tian Xia, and Xun Gu. A computational analysis framework for molecular cell dynamics: Case-study of exocytosis. *PLOS ONE*, 7(7):1–10, 07 2012.

[8] Yolanda Gimenez-Molina, José Villanueva, Maria del Mar Francés, Salvador Viniegra, and Luis M. Gutiérrez. Multiple mechanisms driving f-actin-dependent transport of organelles to and from secretory sites in bovine chromaffin cells. *Frontiers in Cellular Neuroscience*, 12:344, 2018.

[9] D. Giner, I. López, J. Villanueva, V. Torres, S. Viniegra, and L.M. Gutiérrez. Vesicle movements are governed by the size and dynamics of f-actin cytoskeletal structures in bovine chromaffin cells. *Neuroscience*, 146(2):659 – 669, 2007.

[10] L. M. Gutiérrez and J. Villanueva. The role of F-actin in the transport and secretion of chromaffin granules: an historic perspective. *Pflugers Arch.*, 470(1):181–186, 01 2018.

[11] M.H. Holmes. *Introduction to Perturbation Methods*. Texts in Applied Mathematics. Springer New York, 2012.

[12] Daungruthai Jarukanont, Imelda Bonifas Arredondo, Ricardo Femat, and Martin E. Garcia. Vesicle motion during sustained exocytosis in chromaffin cells: Numerical model based on amperometric measurements. *PLOS ONE*, 10(12):1–25, 12 2015.

[13] Michael Klann, Heinz Koeppl, and Matthias Reuss. Spatial modeling of vesicle transport and the cytoskeleton: The challenge of hitting the right road. *PLOS ONE*, 7(1):1–15, 01 2012.

[14] Guillaume Maucort, Ravikiran Kasula, Andreas Papadopulos, Timo A. Nieminen, Halina Rubinsztein-Dunlop, and Frederic A. Meunier. Mapping organelle motion reveals a vesicular conveyor belt spatially replenishing secretory vesicles in stimulated chromaffin cells. *PLOS ONE*, 9(1):1–9, 01 2014.

[15] Luis S. Mayorga, Meghna Verma, Raquel Hontecillas, Stefan Hoops, and Josep Bassaganya-Riera. Agents and networks to model the dynamic interactions of intracellular transport. *Cellular Logistics*, 7(4):e1392401, 2017.

[16] J. M. Newby and P. C. Bressloff. Quasi-steady state reduction of molecular motor-based models of directed intermittent search. *Bull. Math. Biol.*, 72(7):1840–1866, Oct 2010.

[17] Dietmar Oelz and Alex Mogilner. A drift-diffusion model for molecular motor transport in anisotropic filament bundles. *Discrete & Continuous Dynamical Systems - A*, 36(8):4553–67, 2016.

[18] M. Oheim and W. Stühmer. Tracking chromaffin granules on their way through the actin cortex. *Eur. Biophys. J.*, 29(2):67–89, 2000.

[19] Sergio D. Rosé, Tatiana Lejen, Luciana Casaletti, Roy E. Larson, Teodora Dumitrescu Pene, and José-María Trifaró. Myosins ii and v in chromaffin cells: myosin v is a chromaffin vesicle molecular motor involved in secretion. *Journal of Neurochemistry*, 85(2):287–298, 2003.

[20] Rüdiger Rudolf, Tanja Kögel, Sergei A. Kuznetsov, Thorsten Salm, Oliver Schlicker, Andrea Hellwig, John A. Hammer, and Hans-Hermann Gerdes. Myosin va facilitates the distribution of secretory granules in the f-actin rich cortex of pc12 cells. *Journal of Cell Science*, 116(7):1339–1348, 2003.

[21] D.A. Smith and R.M. Simmons. Models of motor-assisted transport of intracellular particles. *Biophysical Journal*, 80(1):45 – 68, 2001.

[22] J.-M. Trifaró, M.-F. Bader, and J.-P. Doucet. Chromaffin cell cytoskeleton: its possible role in secretion. *Canadian Journal of Biochemistry and Cell Biology*, 63(6):661–679, 1985. PMID: 2994861.

[23] J.-M. Trifaró, S. Gasman, and L. M. Gutiérrez. Cytoskeletal control of vesicle transport and exocytosis in chromaffin cells. *Acta Physiologica*, 192(2):165–172, 2008.

School of Mathematics and Pysics, The University of Queensland, Brisbane, Australia
Email address: d.oelz@uq.edu.au